Research Article | Vol. 10, No. 8 / 1 August 2020 / Optical Materials Express 2011

Optical Materials EXPRESS

Visible emission studies of melt-grown Dy-doped $CsPbCl_3$ and KPb_2Cl_5 crystals

UWE HOMMERICH,[1,*] SAMUEL UBA,[1] A. KABIR,[1] SUDHIR B. TRIVEDI,[2] CLAYTON YANG,[2] AND EI EI BROWN[3]

[1] *Department of Physics, Hampton University, Hampton, VA 23668, USA*
[2] *Brimrose Corporation of America, Sparks Glencoe, MD 21152, USA*
[3] *US Army Research Laboratory, 2800 Powder Mill Rd, Adelphi, MD 20783, USA*
[*] *uwe.hommerich@hamptonu.edu*

Abstract: We report results of the optical properties of Dy-doped $CsPbCl_3$ and KPb_2Cl_5 bulk crystals for potential applications in yellow solid-state laser development. The crystals were synthesized from purified starting materials and melt-grown by vertical Bridgman technique. Optical transmission measurements revealed characteristic absorption bands from intra-4f transitions of Dy^{3+} ions. Direct optical excitation at 455 nm ($^6H_{15/2} \rightarrow {}^4I_{15/2}$) resulted in dominant yellow emission bands at ~575 nm from the $^4F_{9/2}$ excited state of Dy^{3+} ions. In addition, both crystals exhibited weaker emission lines in the blue (~483 nm) and red (~670 nm) regions. The peak emission-cross sections for the yellow transition ($^4F_{9/2} \rightarrow {}^6H_{13/2}$) were determined to be $\sim 0.22 \times 10^{-20}$ cm^2 for Dy: $CsPbCl_3$ ($\lambda_{peak} = 576.5$ nm) and $\sim 0.59 \times 10^{-20}$ cm^2 for Dy: KPb_2Cl_5 ($\lambda_{peak} = 574.5$ nm). The spectral properties and decay dynamics of the $^4F_{9/2}$ excited state were evaluated within the Judd-Ofelt theory to predict total radiative decay rates, branching ratios, and emission quantum efficiencies.

1. Introduction

The visible emission properties of Dy^{3+} doped solids continue to be of current interest for applications in white light source development and yellow solid-state lasers [1–7]. Laser action based on the yellow Dy^{3+} transition $^4F_{9/2} \rightarrow {}^6H_{13/2}$ was first reported at cryogenic temperature for Dy: $KY(WO_4)_2$ and Dy: $KGd(WO_4)_2$ under flashlamp pumping [4]. More recently, blue laser diode pumped Dy^{3+} solid-state lasers were reported for Dy: YAG [6] and Dy,Tb: $LiLuF_4$ [7] operating at room temperature. Ternary lead halides including halide perovskites with composition $CsPbX_3$ (X = Br, Cl) have emerged as promising photonic materials for applications in photovoltaics, optoelectronics, and nuclear radiation detection [8–11]. The low-phonon energy of lead halide based materials has also been of interest for rare earth (RE) doping in solid-state laser applications at IR wavelengths [12–16]. For example, Nd doped KPb_2Br_5 and $RbPb_2Cl_5$ crystals have shown lasing at several near-IR wavelengths [13], whereas Dy doped $RbPb_2Cl_5$ has shown mid-IR lasing at 5.5 µm [15]. The low-phonon energies of lead halide based crystals promises also efficient visible emission from RE ions with only weak non-radiative decay. Furthermore, the relatively broad spectral features observed from RE doped ternary lead halides reduces requirements for wavelength stabilization in diode laser pumping and suggests possible yellow laser tuning. In this paper, we present results of the material preparation and visible emission properties of Dy doped $CsPbCl_3$ and KPb_2Cl_5 crystals melt-grown by vertical Bridgman technique. The visible emission properties were studied and important spectroscopic parameters were derived for applications in yellow laser development.

#398498 https://doi.org/10.1364/OME.398498
Journal © 2020 Received 26 May 2020; revised 28 Jun 2020; accepted 28 Jun 2020; published 31 Jul 2020

Optical Materials EXPRESS

2. Materials and experimental details

$CsPbCl_3$ (CPC) is a direct semiconductor with a bandgap of ~ 3.0 eV. It has a density of 4.21 g/cm^3 and a melting point of ~ 600 °C [16]. CPC crystallizes in a close to cubic perovskite structure. CPC has a low moisture sensitivity and can be handled under ambient conditions. The refractive index was derived from published data to be n~1.75 at visible to near-IR wavelengths [17]. KPb_2Cl_5 (KPC) is a monoclinic crystal with a band gap of ~3.77 eV [18]. KPC has a density of 4.629 g/cm^3 and a melting point of 434 °C [18]. KPC is considered non-hygroscopic and has a refractive index of n~2 [12]. Dy: CPC and Dy: KPC crystals were grown by a vertical Bridgman technique employing a two-zone furnace [14]. Beads of $PbCl_2$ (99.999%) were mixed in a stoichiometric ratio with CsCl (99.999%) or KCl (99.999%) to synthesize CPC or KPC, respectively. $DyCl_3$ was added as dopant to the mix at 1-2 wt%. The combined material was loaded into a pre-cleaned quartz ampoule inside an argon-filled glovebox and heated at ~110 °C under a dynamic vacuum for 2 days. After sealing under vacuum (~10^{-6} torr) the growth ampoule was positioned inside the hot zone of a two-zone crystal growth furnace. The temperature of the hot zone was kept at ~30 °C above the melting point. The ampoule was then lowered at a growth speed of 1-3 mm/h. After the crystal growth was completed, the furnace temperature was slowly reduced to room-temperature over a time period of four days. Single crystalline grains in the size range of 5 to 10 mm could be mined out from each boule. It was observed that Dy: KPC was colorless and stable under ambient conditions without any change in overall transmission. In contrast, the Dy: CPC crystal exhibited a slight yellowish coloration and became milky with reduced transmission after a few hours of exposure to air. The crystal structure of CPC and KPC was confirmed by XRD measurements. The dopant concentration for Dy: CPC was measured to be 1.1×10^{20} cm^{-3} using inductively coupled plasma optical emission spectroscopy (ICP-OES). The Dy concentration for Dy: KPC was determined to be 5×10^{19} cm^{-3} by comparison to published absorption cross-section data [12]. Samples of good optical quality with dimensions of ~5×5×3 mm^3 were selected and polished for spectroscopic studies. Transmission spectra were measured using a Shimadzu UV-3600 spectrophotometer. Emission spectra, excitation spectra, and lifetimes were recorded employing an Edinburgh Instruments FLS 980 fluorescence spectrometer.

3. Results and discussion

3.1. Transmission, absorption, and Judd-Ofelt analysis

The optical transmission and absorption spectra of Dy: CPC and Dy: KPC crystals are shown in Figs. 1 and 2. For both crystals the transmission in the IR region was over 50%, but decreased significantly at visible wavelengths due to background absorption losses.

Characteristic intra-4f absorption bands of Dy^{3+} ions were identified in the IR region peaking at ~0.76, ~0.81, ~0.91, ~1.10, ~1.29, ~1.67, and ~2.9 µm corresponding to transitions from the $^6H_{15/2}$ ground state to the $^6F_{3/2}$, $^6F_{5/2}$, $^6F_{7/2}$, $^6H_{7/2}$+$^6F_{9/2}$, $^6H_{9/2}$+$^6F_{11/2}$, $^6H_{11/2}$, and $^6H_{13/2}$ states, respectively. In addition, weaker UV-visible absorption bands were observed for Dy: KPC at 354 nm ($^6P_{7/2}$), 366 nm ($^6P_{5/2}$), 388 nm ($^4I_{13/2}$), 427 nm ($^4G_{11/2}$), 454 nm ($^4I_{15/2}$), and 476 nm ($^4F_{9/2}$), respectively [19,20]. Dy: CPC did not reveal any visible Dy^{3+} absorption bands most likely due to overlapping defects and the onset of near bandedge absorption [16]. Using five IR Dy^{3+} absorption bands a Judd-Ofelt (JO) analysis was performed for Dy: CPC. The 2.9 µm absorption band was not included because of possible overlap with OH absorption [14]. The reduced matrix elements were taken from Kaminskii [19] and yielded the following intensity parameters: $\Omega_2 = 4.05 \times 10^{-20}$ cm^2, $\Omega_4 = 0.06 \times 10^{-20}$ cm^2, and $\Omega_6 = 0.39 \times 10^{-20}$ cm^2. Table 1 summarizes the relevant data and calculated oscillator strengths for Dy: CPC. For Dy: KPC a JO analysis was reported by Nostrand et al. [12] yielding the intensity parameters: $\Omega_2 = 5.41 \times 10^{-20}$ cm^2, $\Omega_4 = 0.99 \times 10^{-20}$, $\Omega_6 = 2.96 \times 10^{-20}$ cm^2.

Optical Materials EXPRESS

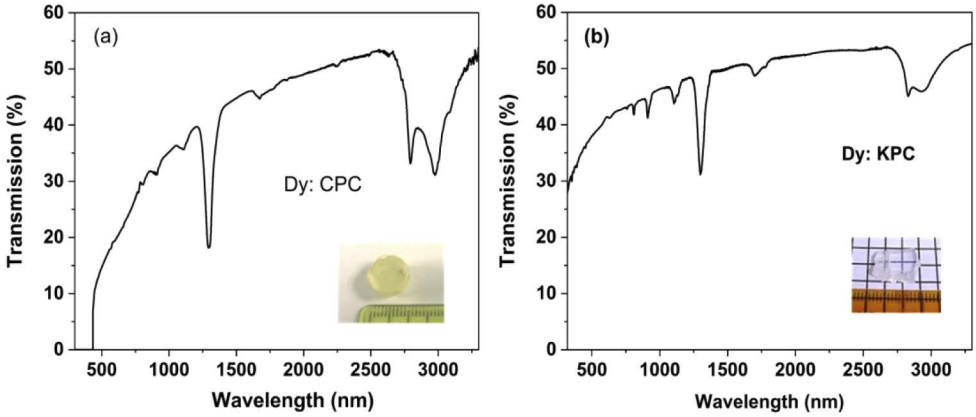

Fig. 1. Room temperature transmission spectra and pictures (a) Dy:CPC and (b) Dy: KPC.

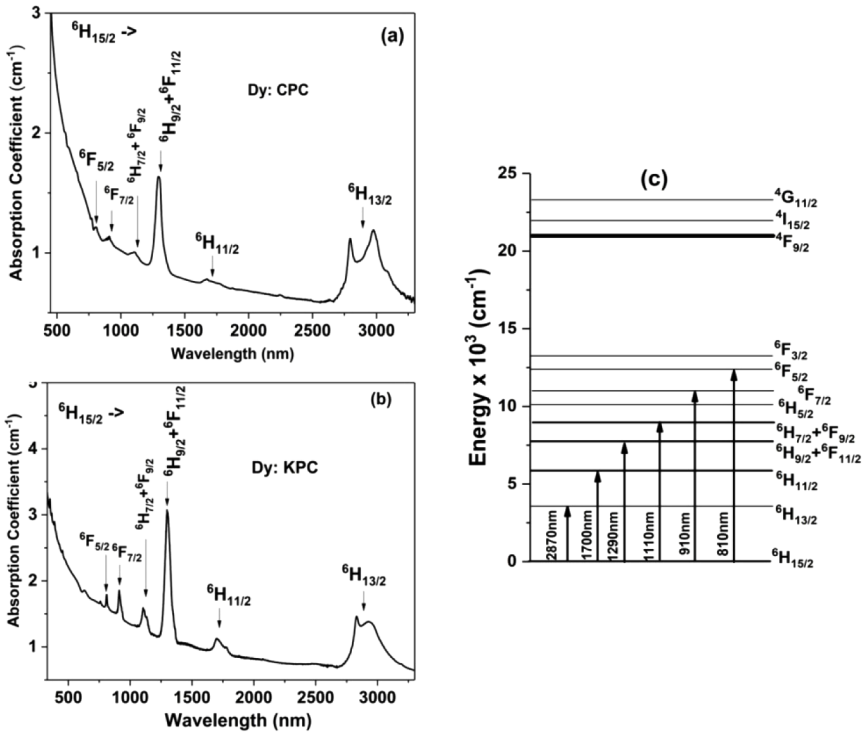

Fig. 2. Room temperature absorption coefficient spectra for (a) Dy: CPC and (b) Dy: KPC. IR transitions originating from the $^6H_{15/2}$ ground state of Dy^{3+} are indicated in the figure and are shown in (c).

3.2. Visible emission studies and emission cross-sections

Figure 3 depicts the room temperature visible emission spectra of Dy: CPC and Dy: KPC under 455 nm optical pumping into the $^6H_{15/2} \rightarrow {}^4I_{15/2}$ absorption transition. Both crystals exhibited dominant yellow emission bands from the $^4F_{9/2} \rightarrow {}^6H_{13/2}$ transition at 576.5 nm (FWHM: 9.5 nm) for Dy: CPC and 574.5 nm (FWHM: 9.1 nm) for Dy: KPC, respectively. Other observed Dy^{3+} emission lines originating from the $^4F_{9/2}$ level showed peak wavelengths at 482.6 ($^4F_{9/2}$

Optical Materials EXPRESS

Table 1. Absorption transitions, average absorption wavelengths, integrated absorption coefficients, experimental line strengths, and calculated line strengths values for Dy: CPC.

Transition $^6H_{15/2} \rightarrow$	Average Wavelength (μm)	$\int \alpha(\lambda)d\lambda$ (μm/cm)	S^{ed}(exp) ($x10^{-20}cm^2$)	S^{ed}(calc) ($x10^{-20}cm^2$)
$^6H_{11/2}$	1.67	0.0071	4.02	5.21
$^6H_{9/2} + {}^6F_{11/2}$	1.29	0.0497	3.72	3.73
$^6H_{7/2} + {}^6F_{9/2}$	1.10	0.0030	2.91	3.12
$^6F_{7/2}$	0.91	0.0032	3.56	2.81
$^6F_{5/2}$	0.81	0.0019	1.42	2.36

$\rightarrow {}^6H_{15/2}$), 668.6 ($^4F_{9/2} \rightarrow {}^6H_{11/2}$), and 755.0 nm ($^4F_{9/2} \rightarrow {}^6H_{9/2}$+$^6F_{11/2}$) for Dy: CPC. The corresponding emission lines for Dy: KPC peaked at the wavelengths of 482.9, 663.7, and 752.5 nm.

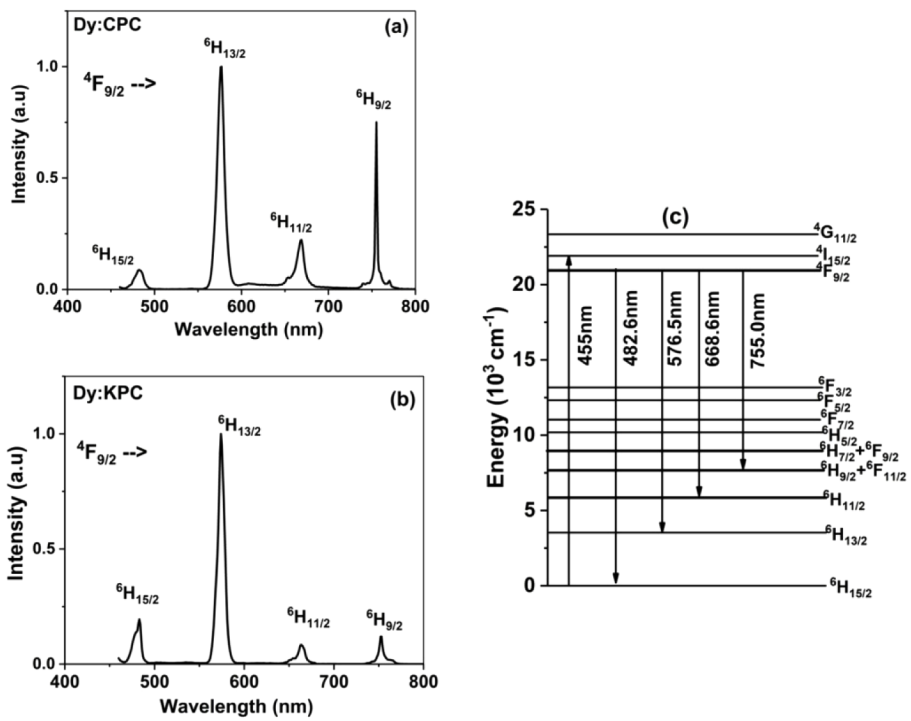

Fig. 3. Room temperature emission spectra under 455 nm excitation for (a) Dy: CPC and (b) Dy: KPC. An energy level diagram showing the relevant emission lines from the $^4F_{9/2}$ excited states for Dy: CPC is depict under (c). All emission data are summarized in Table 2.

The excitation spectra for Dy: CPC and Dy: KPC for a monitor wavelength of ~575 nm are shown in Fig. 4. It can be seen that intra-4f excitation at ~455 nm ($^6H_{15/2} \rightarrow {}^4I_{15/2}$) is the most efficient pump wavelength for achieving yellow emission from both crystals. The excitation spectra also reveal that carrier-mediated excitation using above gap energies does not efficiently excite Dy^{3+} ions in both hosts. The room temperature $^4F_{9/2}$ emission decay transients monitored at ~575 nm for Dy: CPC and Dy: KPC are shown in Fig. 5. For lifetime studies low-concentration samples (~0.5 wt%) were employed to avoid possible cross-relaxation processes [3]. Following

Optical Materials EXPRESS

Table 2. Observed peak emission wavelengths (λ_p), calculated radiative decay rates (A) and branching ratios (β) for the $^4F_{9/2}$ excited state of Dy^{3+} in $CsPbCl_3$ and KPb_2Cl_5. Calculated (τ_{rad}) and measured (τ_{exp}) lifetimes are also given in the table. The reduced matrix elements for JO-analysis were taken from Ref. [22].

Transition $^6F_{9/2} \rightarrow$	Dy: CPC			Dy: KPC		
	λ_p (nm)	A (s^{-1})	β (%)	λ_p (nm)	A (s^{-1})	β (%)
$^6F_{3/2}$	-	0.02	0	-	0.2	0.01
$^6F_{5/2}$	-	5.9	1.0	-	13.3	0.60
$^6F_{7/2}$	-	0.8	0.14	-	8.3	0.37
$^6H_{5/2}$	-	0.3	0.05	-	5.2	0.23
$^6H_{7/2}$+$^6F_{9/2}$	-	6.2	1.1	-	43.1	1.9
$^6H_{9/2}$+$^6F_{11/2}$	755.0	22.0	3.9	752.5	75.3	3.4
$^6H_{11/2}$	668.6	50.4	8.8	663.7	130.1	5.8
$^6H_{13/2}$	576.5	445.8	77.9	574.5	1454.1	65.1
$^6H_{13/2}$	482.6	39.7	6.9	482.9	497	22.2
Decay times		τ_{rad}=1.75 ms			τ_{rad}=0.45 ms	
		τ_{exp}=1.0 ms			τ_{exp}=0.37 ms	

an initial fast decaying component, the emission lifetime of Dy: CPC was single exponential with a value of ~1.0 ms. The initial fast decaying component is attributed to residual broad background emission from the CPC host. Since the decay time for Dy: KPC was slightly non-exponential, the average lifetime was determined according to the following equation:

$$\tau_{avg} = \int t \cdot I(t)dt / \int I(t)dt \tag{1}$$

where I (t) is the emission intensity as a function of time. The average lifetime for Dy: KPC yielded a value of 0.37 ms.

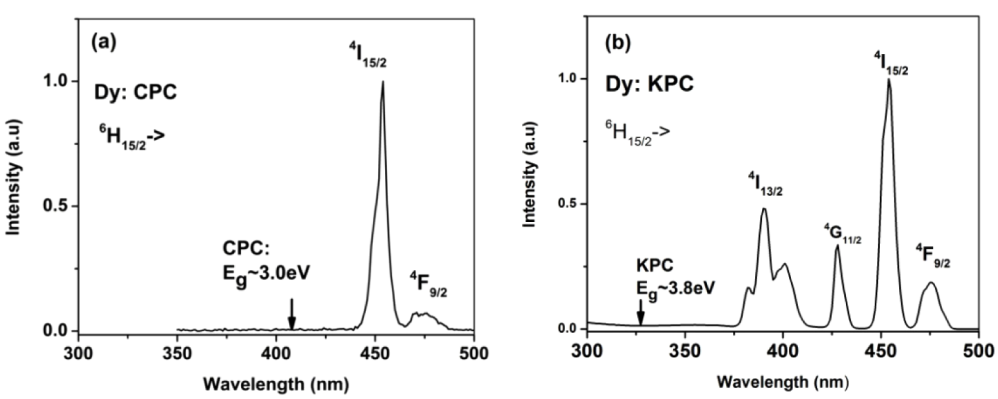

Fig. 4. Excitation spectra for (a) Dy: CPC and (b) Dy: KPC. The emission was monitored at ~575 nm. The bandedge energies of both crystals are indicated in the figures.

Based on the existing emission data, the peak emission cross-sections were calculated using the Fuchtbauer-Ladenburg expression [5]:

$$\sigma_p = \frac{\lambda_{peak}^4 \beta}{8\pi n^2 c \tau_{rad} \Delta\lambda_{eff}} \tag{2}$$

Optical Materials EXPRESS

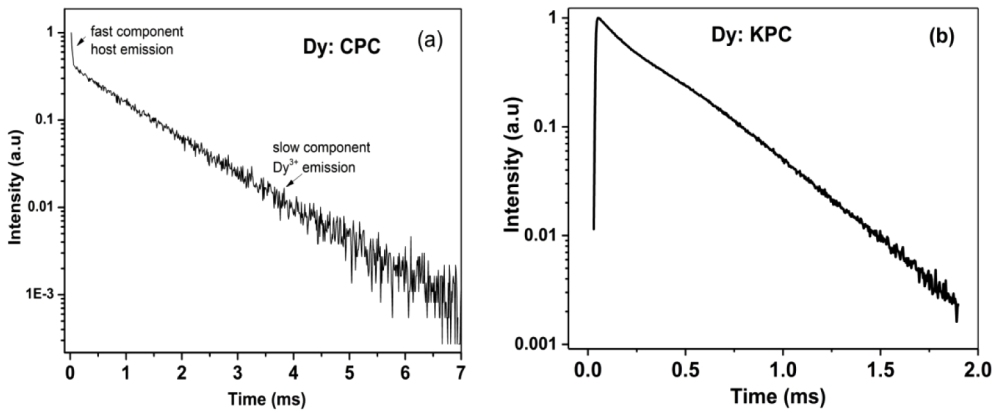

Fig. 5. Room temperature yellow emission lifetime ($^4F_{9/2} \rightarrow {}^6H_{13/2}$) under 455 nm excitation for (a) Dy: CPC and (b) Dy: KPC. The emission was monitored at ~575 nm.

where λ_{peak} is the peak emission wavelength, β is the branching ratio, τ_{rad} is the radiative lifetime, and $\Delta\lambda_{eff}$ is the emission bandwidth. The derived peak emission cross-sections for Dy: CPC and Dy: KPC were determined to be 0.22×10^{-20} cm^2 ($\lambda_{peak} = 576.5$ nm) and 0.59×10^{-20} cm^2 ($\lambda_{peak} = 574.5$ nm), respectively. The cross-section spectra for both crystals are shown in Fig. 6 and the emission properties are summarized in Table 2. It can be noted, that the calculated and experimental emission lifetimes are similar for Dy: KPC, which suggest a quantum efficiency of ~82%. Since KPC has a small maximum phonon energy of only $h\omega_{max}$ ~200 cm^{-1} and due to the large energy-separation of ~7200 cm^{-1} between the $^4F_{9/2}$ and the next lower $^4F_{1/2}$ level, non-radiative decay through multi-phonon relaxation is expected to be weak [5,19]. For Dy: CPC measured and calculated lifetimes are significantly different, which indicates the existence of non-radiative decay despite the narrow phonon spectrum ($h\omega_{max}$ ~375 cm^{-1}) of the host. Non-radiative losses in Dy: CPC are most likely due to residual defects as indicated by the significant background absorption and OH related multi-phonon quenching [16,21]. Further studies on the relation between decay dynamics and material purification are in progress.

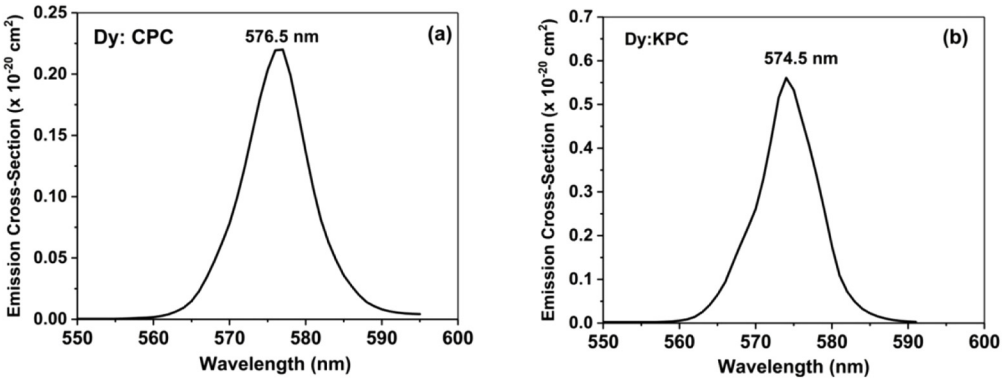

Fig. 6. Yellow emission cross-section spectra for the ($^4F_{9/2} \rightarrow {}^6H_{13/2}$) transition (a) Dy: CPC and (b) Dy: KPC.

The main laser relevant spectroscopic parameters for the investigated Dy: CPC and Dy: KPC in comparison to other Dy doped crystals are shown in Table 3. It can be noted that Dy: KPC compares well with Dy: YAG and Dy: $LiLuF_4$ laser materials and exhibits higher emission

Optical Materials EXPRESS

cross-section and quantum efficiency. Furthermore, the broad absorption and emission features with bandwidth of several nanometers offer advantages for diode laser pumping and yellow laser tunability. Careful studies on possible quenching effects for higher Dy^{3+} concentrations, however, are still needed to fully explore Dy: KPC as a novel yellow laser material. For Dy: CPC the strong background absorption losses due to intrinsic defects severely limits its potential for laser applications.

Table 3. Peak emission wavelength (λ_p), peak emission cross-section (σ_p), emission lifetime (τ), emission quantum efficiency (η), and branching ratio (β) for different Dy doped crystals at 300 K.

Host Crystal	λ_p (nm)	σ_p (x10^{-20}cm^2)	τ_{exp} (ms)	η (%)	β (%)
KPb_2Cl_5	574.5	0.59	0.37	82.2	65.1
$CsPbCl_3$	576.5	0.22	1.0	57.1	77.9
YAG [6]	582.7	0.41	0.67	~33	50.9
$LiLuF_4$ [7,23]	~574	~0.46	~1.3	16.6	65.4
CeF_3 [24]	569	0.93	1.53	40.8	63.7

4. Conclusions

Results of the material preparation and optical spectroscopy for Dy: $CsPbCl_3$ and Dy: KPb_2Cl_5 were presented. High purity starting materials were employed for the synthesis of both compounds and crystal growth experiments were carried out using vertical Bridgman technique. Under resonant excitation into an intra-4f absorption band, Dy: CPC and Dy: KPC exhibited bright yellow emission peaking in the ~575-577 nm range from the $^4F_{9/2} \rightarrow {}^6H_{13/2}$ transition of Dy^{3+} ions. Based on a Judd-Ofelt analysis, it was determined that the yellow emission exhibited high branching ratios (65-78%) with an emission quantum efficiency of ~82% for Dy: KPC. In addition, Dy: KPC also exhibited a slightly higher peak emission cross-section for the $^4F_{9/2} \rightarrow {}^6H_{13/2}$ transition compared to other yellow laser crystals [6,7], which indicates the potential of Dy: KPC for solid-state gain media applications. On the contrary, Dy: CPC exhibited non-radiative losses due to unknown defects and possible OH multi-phonon relaxation. Dy: CPC also suffered from intrinsic transmission losses which make this material less attractive for visible laser applications. Future studies on these crystals will focus on additional purification experiments in an effort to reduce background absorption losses and to improve overall crystal quality.

Funding

National Science Foundation (DMR-PREM-1827820); Army Research Office (W911NF1810447).

Disclosures

The authors declare no conflicts of interest.

References

1. Z. Zhang, J. Li, W. Wang, G. Duan, W. Zhao, and Z. Liu, "Luminescence Properties of Dy^{3+} doped $Gd_2(WO_4)_3$ Phosphor Prepared by Hydrothermal Method," IOP Conf. Ser.: Mater. Sci. Eng. **389**, 012019 (2018).
2. E. Cavalli, "Optical spectroscopy of Dy^{3+} in crystalline hosts: General aspects, personal considerations and some news," Opt. Mater. X **1**, 100014 (2019).
3. G. Dominiak-Dzik, P. Solarz, W. Ryba-Romanowski, E. Beregi, and L. Kovacs, "Dysprosium-doped $YAl_3(BO_3)_4$ (YAB) crystals: an investigation of radiative and non-radiative processes," J. Alloys Compd. **359**(1-2), 51–58 (2003).
4. A. A. Kaminskii, U. Hömmerich, D. Temple, J. T. Seo, K. Ueda, S. Bagayev, and A. A. Pavlyulk, "Visible Laser Action of Dy^{3+} in Monoclinic $KY(WO_4)_2$ and $KGd(WO_4)_2$ crystal under Xe-flashlamp pumping," Jap. J. Appl. Phys. **39**(Part 2, No. 3A/B), L208–L211 (2000).

Optical Materials EXPRESS

5. A. Kaminskii A, B. Gruber J, N. Bagaev S, K. Ueda, U. Hommerich, T. Seo J, D. Temple, B. Zandi, A. Kornienko A, B. Dunina E, A. Pavlyuk A, F. Klevtsova R, and A. Kuznetsov F, "Optical spectroscopy and visible stimulated emission of Dy^{3+} ions in monoclinic $KY(WO_4)_2$ and $KGd(WO_4)_2$ crystals," Phys. Rev. B **65**(12), 125108 (2002).
6. S. R. Bowman, S. O'Connor, and N. J. Condon, "Diode pumped yellow dysprosium lasers," Opt. Express **20**(12), 12906–12911 (2012).
7. G. Bolognesi, D. Parisi, D. Calonico, G. A. Costanzo, F. Levi, P. W. Metz, C. Krankel, G. Huber, and M. Tonelli, "Yellow laser performance of Dy^{3+} in co-doped Dy, Tb: $LiLuF_4$," Opt. Lett. **39**(23), 6628–6631 (2014).
8. R. Babu, L. Giribabu, and S. P. Singh, "Recent Advances in Halide-Based Perovskite Crystals and Their Optoelectronic Applications," Cryst. Growth Des. **18**(4), 2645–2664 (2018).
9. H. H. Ma, M. Imran, Z. Dang, and Z. Hu, "Growth of Metal Halide Perovskite, from Nanocrystal to Micron-Scale Crystal: A Review," Crystals **8**(5), 182 (2018).
10. C. C. Stoumpos, C. D. Malliakas, J. A. Peters, Z. Lui, M. Sebastian, J. Im, T. C. Chasapis, A. C. Wibowo, D. Y. Chung, A. J. Feeman, B. C. Wessels, and M. G. Kanatzidis, "Crystal Growth of the Perovskite Semiconductor $CsPbBr_3$: A new Material for High-Energy Radiation Detection," Cryst. Growth Des. **13**(7), 2722–2727 (2013).
11. D. N. Dirin, I. Cheniukh, S. Yakunin, Y. Shynkarenko, and M. V. Kovalenko, "Solution-Grown $CsPbBr_3$ Perovskite Single Crystals for Photon Detection," Chem. Mater. **28**(23), 8470–8474 (2016).
12. M. C. Nostrand, R. H. Page, S. A. Payne, L. I. Isaenko, and A. P. Yelisseyev, "Optical Properties of Dy^{3+} and Nd^{3+} doped KPb_2Cl_5," J. Opt. Soc. Am. B **18**(3), 264–275 (2001).
13. K. Rademaker, E. Heuman, G. Huber, S. A. Payne, W. F. Krupke, L. I. Isaenko, and A. Burger, "Laser Activity at 1.18,1.07, and 0.97 (m in the low-phonon-energy hosts KPb_2Br_5 and $RbPb_2Br_5$ doped with Nd^{3+}," Opt. Lett. **30**(7), 729–731 (2005).
14. U. Hommerich, E. Brown, A. Kabir, D. Hart, S. B. Trivedi, F. Jin, and H. Chen, "Crystal growth and characterization of undoped and Dy-doped $TlPb_2Br_5$ for infrared lasers and nuclear radiation detection," J. Cryst. Growth **479**, 89–92 (2017).
15. A. G. Okhrimchuk, L. N. Butvina, E. M. Dianov, I. A. Shestakova, N. V. Lichkova, V. N. Zagorodney, and A. Shestakov, "Optical spectroscopy of the $RbPb_2Cl_5$: Dy^{3+} laser crystal and oscillation at 5.5 (m at room temperature," J. Opt. Soc. Am. B **24**(10), 2690–2695 (2007).
16. M. Kobayashi, K. Omata, S. Sugimoto, Y. Tamagawa, T. Kuroiwa, H. Asada, H. Takeuchi, and S. Kondo, "Scintillation characteristics of $CsPbCl_3$ single crystals," Nucl. Instrum. Methods Phys. Res., Sect. A **592**(3), 369–373 (2008).
17. N. Pandey, A. Kumar, and S. Chakrabarti, "Investigation of the structural, electronic, and optical properties of Mn-doped $CsPbCl_3$: theory and experiment," RSC Adv. **9**(51), 29556–29565 (2019).
18. L. Isaenko, A. Yelisseyev, A. Tkachuk, and S. Ivanova, (2008) New Monocrystals with Low Phonon Energy for Mid-IR Lasers, In: M. Ebrahim-Zadeh and I. T. Sorokina, eds. *Mid-Infrared Coherent Sources and Applications. NATO Science for Peace and Security Series B: Physics and Biophysics*, Springer, Dordrecht.
19. A. A. Kaminskii, *Crystalline lasers: Physical processes and operating schemes*, CRC press, New York (1996).
20. L. Fang, X. Zhou, J. Zhang, H. Xia, B. Chen, and H. Song, "Control of white light emission via co-doping of Dy^{3+} and Tb^{3+} ions in $LiLuF_4$ single crystals under UV excitation," J. Mater. Sci.: Mater. Electron. **31**(4), 3405–3414 (2020).
21. K. Watanabe, M. Koshimizu, T. Yanagida, Y. Fujimoti, and K. Asai, "Luminescence and scintillation properties of La-and La,Ag-doped $CsPbCl_3$ single crystals," Jpn. J. Appl. Phys. **55**(2S), 02BC20 (2016).
22. C. K. Jayasankar and E. Rukmini, "Spectroscopic investigation of Dy^{3+} ions in borosulphate glasses," Phys. B **240**(3), 273–288 (1997).
23. S. Bigotta, M. Tonelli, E. Cavalli, and A. Belletti, "Optical spectra of Dy^{3+} in KY_3F_{10} and $LiLuF_4$ crystalline fibers," J. Lumin. **130**(1), 13–17 (2010).
24. Y. Yang, L. Zhang, S. Li, S. Zhang, M. He, M. Xu, and Y. Hing, "Crystal growth and 570 nm emission of Dy^{3+} doped CeF_3 single crystal," J. Lumin. **215**, 116707 (2019).